Study On the Optimal Layout Method for Multibeam Bathymetry Based on Dynamic Programming

Shiting Feng [1], Zijing Li [1], Yulun Wu [2], Penghui Zhu [1, *]

[1] School of Computer Science and Technology, Shandong University of Technology, Zibo, China, 255000

[2] School of Chemistry and Chemical Engineering, Shandong University of Technology, Zibo, China, 255000

* Corresponding Author Email: 18806338294@163.com

Abstract. Multibeam sonar technology is widely used in fields such as marine science. Compared to single-beam systems, it offers greater coverage and precision. However, the coverage width and overlap rate are easily influenced by factors such as water depth, opening angle, and seabed slope, which in turn affect data acquisition accuracy and efficiency. Specifically, this study employs the sine theorem and principles from plane geometry to develop mathematical models for bathymetry in sloping submarine environments. A method for determining survey line coverage width in these areas is also proposed. In terms of maritime area network planning, an objective framework is established to compare various network configurations within known seabed topography, identifying the optimal layout. Using a dynamic programming algorithm for model solving, this paper finds that when the survey ship travels north-south, conducting 34 surveys with unequal spacing, the adjacent overlap rate between survey lines can be maintained at 10% to 11%, with the shortest total survey line length being 125,936 meters. The effectiveness of the proposed models is validated through comprehensive evaluation metrics and error band analyses.

Keywords: Law of Sines, Plane Geometry, Objective Planning, Dynamic Programming.

1. Introduction

Multibeam sonar technology, as a high-precision method for underwater topographic mapping, has seen widespread application in recent years across fields such as marine science, resource exploration, channel surveying, and underwater archaeology. Compared to single-beam sonar, multibeam sonar systems can provide a wider coverage area and denser point cloud data, offering unprecedented possibilities for the accurate characterization of seabed topography. However, as factors such as water depth, sonar opening angle, and seabed slope vary, the coverage width of multibeam sonar and the overlap rate between survey lines also change accordingly, directly affecting data acquisition accuracy and coverage efficiency. Yu et al. laid the foundation for the construction of the multibeam model in this paper [1-4]. Existing research provides the theoretical foundation for the construction mechanism of the multi-objective planning model in this paper [5-7]. Wang et al. provide the theoretical basis for the assessment of multibeam bathymetric detection accuracy and the wiring scheme in this paper [8]. Fu et al. provide the theoretical basis for simulating seabed topography data in this paper [9]. Mu et al. provide the theoretical mechanisms for establishing the model for solving optimal solutions using dynamic programming [10].

This study first creates a bathymetric model of a sloping seabed based on the sine theorem and principles of plane geometry, calculating the coverage width for different survey line directions and slopes. Next, when conducting multibeam measurements in unknown sea areas, the paper pre-arranges two distinct line arrangement methods to simulate regions with varying seabed slopes, develops a multi-objective planning model, and conducts simulation experiments. Additionally, an optimal survey line placement algorithm for unknown seabed areas is proposed, incorporating concepts from dynamic programming. Finally, the models developed in this study are applied to actual maritime areas, where area zoning and related indicators are solved.

2. Computational Model for Coverage Width and Overlap Rate in Multibeam Bathymetry

The data in this paper is sourced from www.mcm.edu.cn.

2.1. Coverage Width Measurement Model

The coverage width of multibeam bathymetry is W, the depth of seawater is D, the opening angle of the Multibeam line transducer is θ, and the overlap rate is η. Since the sea bottom surface has a certain inclination, it is necessary to define the distance between neighboring survey lines in the expression of the coverage width as well as overlap rate as their projection on the sea bottom slope [1-4]. At the same time, the coverage width W of the Multibeam bathymetric strip is divided into left-touch beam coverage width W^L and right-touch beam coverage width W^R, as shown in Figure 1. The coverage width of the multibeam survey line is shown in Figure 1, where the slope of the seabed slope is α, according to the equality of the angle of the internal error between the two parallel lines, it can obtain $\angle PAB = \alpha$.

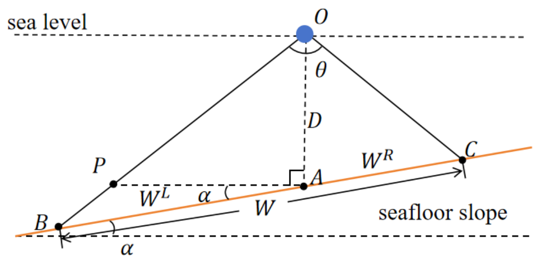

Figure 1. Coverage width schematic.

In $Rt\Delta$OAP, by the sine theorem:

$$\frac{AP}{\sin\angle POA} = \frac{AO}{sin\angle OPA} \tag{1}$$

In $Rt\Delta$PBA, by the sine theorem:

$$\frac{AB}{sin\angle BPA} = \frac{AP}{sin\angle PBA} \tag{2}$$

Associative expression(1), (2), then:

$$AB = \frac{sin\angle BPA}{sin\angle PBA} \cdot AP = \frac{sin\angle BPA}{sin\angle PBA} \cdot \frac{sin\angle POA}{sin\angle OPA} \cdot AO \tag{3}$$

According to the definition of the left-contact beam coverage width, it can be obtained:

$$W^L = \frac{\sin\frac{\theta}{2}}{\cos(\frac{\theta}{2} + \alpha)} \cdot D \tag{4}$$

Similarly:

$$W^R = \frac{sin(\frac{\theta}{2})}{\cos(\frac{\theta}{2} - \alpha)} \cdot D \tag{5}$$

Associative expression(4), (5), the mathematical model between the width of the survey line coverage and the depth of seawater at the center of the sea area is finally established:

$$W = W^L + W^R = \left(\frac{\sin\frac{\theta}{2}}{\cos(\frac{\theta}{2}+\alpha)} + \frac{\sin(\frac{\theta}{2})}{\cos(\frac{\theta}{2}-\alpha)}\right)D \tag{6}$$

2.2. Overlap Rate Measurement Model

The following model provides a method for calculating the overlap rate in practical scenarios: the central point of the sea area is designated as the reference point, with the right side considered as the positive direction. The spacing between two neighboring lines is d. The distance from the reference point to the measurement line is denoted as $R_i(i = 1,2,3,\dots)$. The depth of seawater at the right-hand line point is $D_i(i = 1,2,3,\dots)$. The adjacent lines in the positive directions at the center of the sea area are shown in Figure 2.

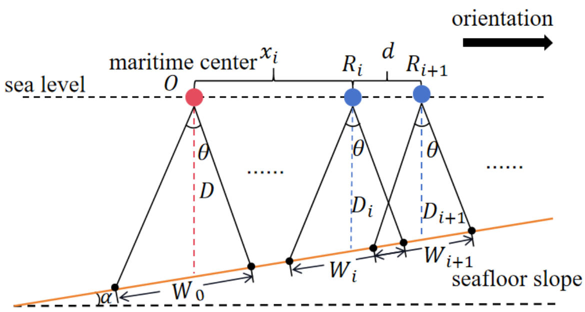

Figure 2. Line charts in the positive direction of the center point of the sea area.

The mathematical model relating the depth of seawater at that point to the depth of seawater at the sea center can be established.

$$D_i = D - x_i \cdot \tan\alpha \qquad (i = 1,2,3\dots) \tag{7}$$

It can be obtained:

$$W_i = W_i^L + W_i^R = \left(\frac{\sin\frac{\theta}{2}}{\cos(\frac{\theta}{2}+\alpha)} + \frac{\sin(\frac{\theta}{2})}{\cos(\frac{\theta}{2}-\alpha)}\right)D_i \tag{8}$$

$$\eta_i = \frac{1 - \frac{d}{\tan\alpha}}{W_{i+1}} \tag{9}$$

2.3. Model Checking

If the seabed plane is inclined to a certain extent, when the slope is 1.5°, the opening angle of the multibeam transducer is 120°, and the depth of seawater at the center point of the sea area is 70m. By utilizing the established multibeam bathymetry system, the measurement model for coverage width and repetition rate between adjacent strips can be solved. The resulting index values are presented in Model test results, as shown in Table 1:

Table.1. Model test results

Distance of the line from the center point /m	Depth of sea /m	Coverage width /m	Overlap with previous line/%
-800	90.949	315.813	——
-600	85.712	297.628	35.695
-400	80.474	279.442	31.511
-200	75.237	261.256	26.743
0	70.000	243.070	21.262
200	64.763	224.885	14.895
400	59.526	206.699	7.407
600	54.289	188.513	-1.525
800	49.051	170.327	-12.365

3. Coverage Width Calculation Model under Multiple Survey Line Directions

The center point of the sea area with different measurement line direction is shown in Figure 3. The survey vessel transmits a multibeam survey line toward the seafloor slope at an angle of $\beta,\ \beta_1,\ \beta_2 ...$ in the direction of the survey line; the angle of intersection of the horizontal plane with the seafloor slope and the direction of the survey line is $\gamma_i(\ i = 1,2,3, \ldots\ )$; and the initial slope is α. With the change of the angle of the measurement line direction, the corresponding relative slope is changed accordingly.

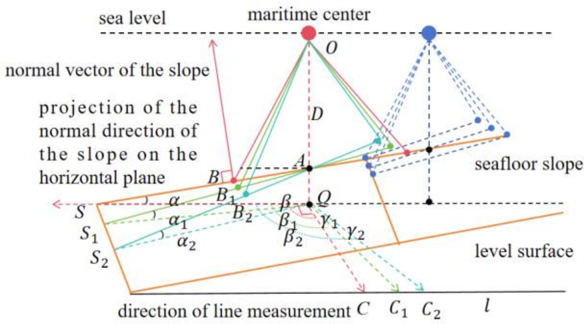

Figure 3. Schematic representation of different line orientations at a given distance in the sea area.

Let the projection of the center point of the sea area on the seabed slope be at a distance from the horizontal $AQ = h$.

In $Rt\Delta$AQS, we have:

$$SQ = h \cdot \tan\alpha \tag{10}$$

In $Rt\Delta QSS_1$, Let γ_1 be the angle between the line intersecting the horizontal plane and the submarine slope and the direction of the survey line, then we have:

$$\cos\gamma_1 = \frac{SQ}{S_1Q} \tag{11}$$

$$S_1Q = \frac{h}{\tan\alpha\cos\gamma_1} \tag{12}$$

In $Rt\Delta$AQS$_1$, according to the tangent function.

$$\frac{h}{S_1Q} = \tan\alpha_1 \tag{13}$$

Associative expression (10)~(13), it is obtained by eliminating the unknown h using the elimination method.

$$\tan\alpha_1 = \tan\alpha\cos\gamma_1 \quad (14)$$

In Figure 3, to calculate the width of survey line coverage at varying distances from the center of the sea area, the relative slope at the survey vessel is initially ascertained. Finally, establish a measurement model for arbitrary positions within the maritime area.

$$W_i = W_i^L + W_i^R = \left(\frac{sin\frac{\theta}{2}}{cos\left(\frac{\theta}{2}+\alpha_i\right)} + \frac{\sin\left(\frac{\theta}{2}\right)}{\cos\left(\frac{\theta}{2}-\alpha_i\right)}\right)(D - x_i\cdot\tan\alpha_i) \quad (15)$$

$$\alpha_i = \arctan(\tan\alpha\cos\gamma_i) \quad (16)$$

Where the value of γ_i is divided into four cases:

(1) when $0 \le \beta_i < \frac{\pi}{2}, \gamma_i = \frac{\pi}{2} - \beta_i$; (2) when $\frac{\pi}{2} \le \beta_i < \pi, \gamma_i = \beta_i - \frac{\pi}{2}$; (3) when $\pi < \beta_i < \frac{3\pi}{2}, \gamma_i = \beta_i - \pi$; (4) when $\frac{3\pi}{2} < \beta_i < 2\pi, \gamma_i = 2\pi - \beta_i$.

4. Wiring Schemes Based on Multi-Objective Planning

4.1. Multi-Objective Planning Wiring Model

Simulation of the sea area to be tested is a north-south length of 2 nautical miles $(L_1 = 3704m)$, east-west width of 4 nautical miles $(L_2 = 7408m)$ rectangular sea area, the center of the sea depth of $110m$ sea water, the seabed is shallow in the west and east depth and the slope of 1.5°, the sea area to be tested to visualize the geometry of the schematic diagram shown in Figure 4:

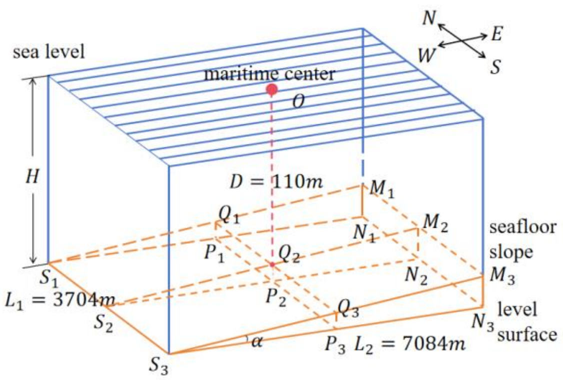

Figure 4. Geometry of the sea area to be surveyed.

Point O is the center of the sea area, here, θ、α、D are known, thus the decision variable is x. The objective function is the shortest total length of the measurement line, and the constraints are the repetition rate between neighboring lines between 10% and 20%, etc., which can be obtained [5-7].

$$\min\sum_{i=1}^{n} d_i = (1 - \eta((\frac{sin\frac{\theta}{2}}{cos\left(\frac{\theta}{2}+\alpha_j\right)} + \frac{\sin\left(\frac{\theta}{2}\right)}{\cos\left(\frac{\theta}{2}-\alpha_j\right)}) \times (D - x_i\cdot tan\,\alpha_j)))\,tan\,\alpha_j \quad (\mathrm{i} = 1,2,3,\ldots;\ \mathrm{j} = 1,2,3,\ldots)$$

$$s.t.\begin{cases} \theta = 120^{\circ} \\ D = 110 \\ d_i > 0 \\ 0.1 < \eta < 0.2 \\ 0 \le x_i < 3542 \\ 0^{\circ} \le \alpha_j < 90^{\circ} \\ 0^{\circ} \le \beta_i < 315^{\circ} \\ \alpha_j = \arctan(\tan\alpha_j \cos(\beta_j - \frac{\pi}{2})) \end{cases} \tag{17}$$

4.2. East-West Wiring and North-South Wiring

Given that the survey vessel lacks prior knowledge of the seafloor topography, various stripes will cover the seafloor slope as the vessel follows a designated survey wiring pattern. This study examines both equal and unequal spacing between survey lines, categorizing the wiring schemes into north-south and east-west wiring to establish a wiring model.

Coverage width visualization in the case of equal spacing of east-west wiring is shown in Figure 5 (a), when the survey ship along the east-west direction for multibeam line, its width W will be constantly decreasing with the measurement of the ship continues to be close to the center point of the sea, and increasing as the measurement of the ship continues to be far away from the center of the sea [8]. It becomes imperative to ensure that the overlap rate between adjacent survey lines in shallow waters does not fall below 10%. While maintaining this condition, it is observed that the overlap rate (η=0.943) between adjacent survey lines in deep water areas significantly surpasses the designated threshold for overlap rate between neighboring lines. Consequently, the east-west wiring scheme is deemed suboptimal under these circumstances.

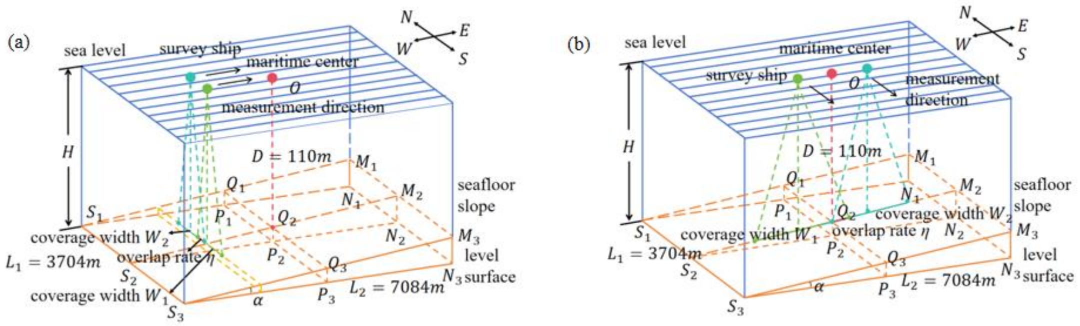

Figure 5. Visualization of east-west and north-south cabling coverage widths. (a) is visualization of east-west cabling coverage widths. (b) is visualization of north-south cabling coverage widths.

The visualization of the unequal spacing coverage width of the north-south oriented cabling is shown in Figure 5 (b). This paper combines the idea of dynamic programming, using Python to solve for the total length of the survey line when the survey ship is traveling along the north-south direction [10]. The solution is obtained when the survey ship traveling along the north-south direction, using unequal spacing measurement wiring, a total of 34 times the north-south direction of the survey line, can be adjacent to the overlap rate between the survey line can be maintained between 10% ~ 11%, the shortest total length of the survey line is 125936m.

In summary, the optimal solution is for the survey ship to measure the wiring along the north-south direction with unequal spacing (In short, route along the line of geometric depth). When the survey ship adopts the north-south unequal spacing survey wiring scheme, the total survey line length is the shortest, and the total survey line length is 125936m.

5. Actual Ocean Bathymetry Solution

5.1. Exploratory Data Analysis and Data Visualization

To enhance measurement accuracy and visualize data, a 3D simulation of seafloor topography was conducted, as shown in Figure 6. The columns represent horizontal coordinates (west to east) and the rows indicate vertical coordinates (south to north). The sea level serves as the zero reference, with darker areas indicating greater depth and lighter areas indicating shallower depth [9].

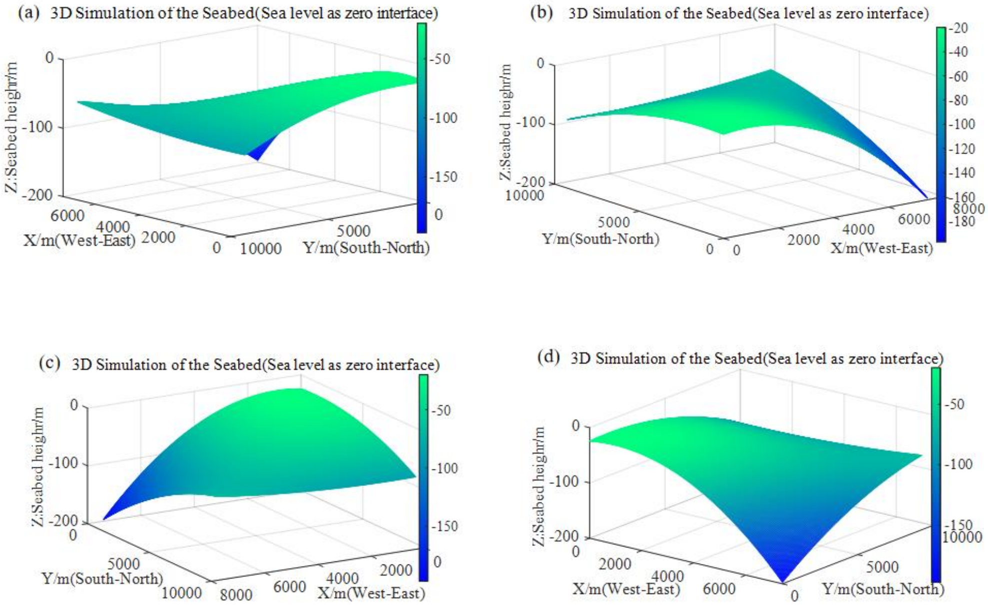

Figure 6. 3D simulation of seafloor topography. (a)~(d) are different perspectives. (a) is a southwestern perspective. (b) is the northwestern perspective. (c) is a northeastern perspective. (d) is a southeastern perspective.

5.2. Polynomial Fitting of Seafloor Surfaces

The results of visualizing the effect of fitting the seafloor topography using the polynomial function are shown in Figure 7:

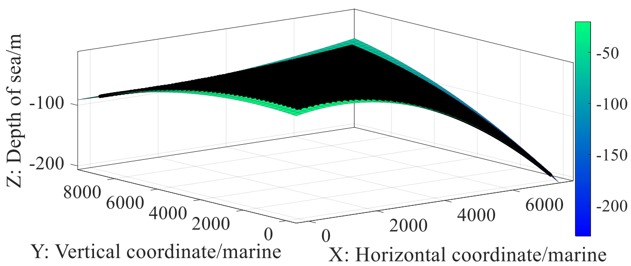

Figure 7. Polynomial function seafloor topographic fit.

5.3. Analysis of Polynomial Fitting Effects

The goodness of fit can be judged by the sum of squared fitting errors (SSE), standard errors ($RMSE$). The polynomial function effectively models the surface, evidenced by a sum of squared errors of 0.4175 and a standard error of 0.0029. Together with other evaluation metrics, these values confirm that the polynomial function fits the surface well.

5.4. Geometric Segmentation of the Sea Area to Be Measured

The targeted sea area is segmented, with the seafloor divided into two slopes of varying inclinations. The area measures 5 nautical miles (9,260 m) long and 4 nautical miles (7,408 m) wide, the seabed topography's three-dimensional geometry is further optimized, as shown in Figure 8.

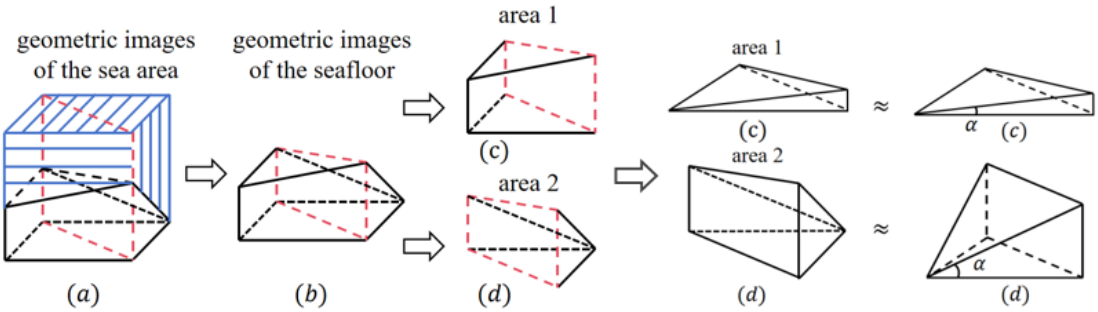

Figure 8. Zoning map of the sea area to be measured.

5.5. Layout of the Trajectory of the Survey Line

The sideline trajectory is established to calculate the total length of the sideline, as illustrated in Figure 9, which presents two scenarios. In the first area and the second area, the line direction is oriented east-west. The survey line trajectories are depicted in Figures 9 (a)~(b).

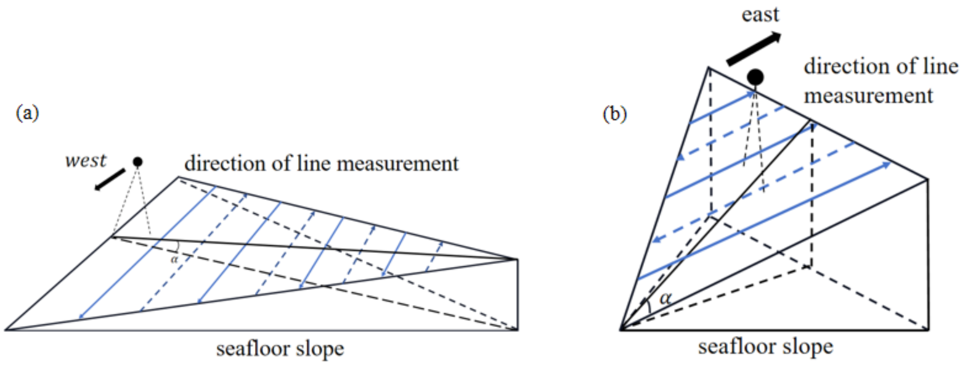

Figure 9. Three-dimensional geometry of seafloor slopes in the subarea. (a) the first scenarios. (b) the second scenarios.

5.6. Model Solution

The model solution is also based on dynamic programming ideas, the two regions obtained were solved, the specific results are in Table of wiring solution results, as shown in Table 2:

Table.2. Table of wiring solution results

Parameter	Number
Total number of lines in the first region	56
Total length of line in first area/m	289280 m
Total number of lines measured in the second region	45
Total length of lines in the second area/m	166680 m
Total length of survey line/m	455960 m
Missed sea area as a percentage of total sea area to be measured/%	1.5 %
Overlap rate over total length/m	28446 m

The missing area is 1.5% of the total, showing effective coverage of the entire sea area.

6. Conclusion

This study uses the sine theorem and plane geometry to create mathematical models for bathymetry in sloping submarine environments, along with a method for calculating survey line coverage width and rate. It presents two wiring schemes for maritime area network planning and establishes a framework for optimal layout using a dynamic programming algorithm. Results show that with the survey ship traveling north-south and conducting 34 surveys with unequal spacing, a 10% to 11% overlap rate can be maintained, resulting in a shortest survey line length of 125,936 meters. The models are applied to actual maritime areas, yielding a total survey line length of 455,960 meters and 1.5% missing area. The effectiveness of the models is validated through evaluation metrics and error analyses.

This paper reveals that multi-objective planning and dynamic programming algorithms effectively address optimal routing in seabed surveying. In the future, wavelet neural networks may predict seabed topography data, supporting the models presented here.

References

[1] Jiacheng Yu, Xueqiang Xu. Terrain inclination correction in multibeam measurement [J]. Heilongjiang Science and Technology Information, 2017(14):9-10.

[2] Linjun Qi, Renjian Zhai, Anping Li. A Multibeam Bathymetry Data Decimation Algorithm Considering Slope and Elevation [J]. Journal of Geo-Information Science, 2023, 25(01): 142-152.

[3] Qiyi Yu. Seabed Topography Measurement Based on Multibeam Bathymetry Technology [J]. Surveying and Spatial Geographical Information, 2022, 45(09): 262-264.

[4] Hui Li, Yanhong Zhan. Application of multibeam bathymetric system in submarine oil and gas pipeline inspection [J]. Petroleum and Chemical Equipment, 2023, 26(11):127-130.

[5] Chengjing Yang, Weihong Shen, Xiaomin Guo. Research on crossing desert strategy based on single-objective linear programming [J]. Modern Information Technology, 2023, 7(01):127-130.

[6] Yi Ni, Jianfeng Yu, et al. Trajectory Planning for Elevator Shaft Drilling Robots Based on Multi-objective Genetic Algorithms [J]. Mechanical and Electronic Engineering, 2023, 41(11): 49-56.

[7] Q.R. Xiong. Research on multi-objective planning model processing based on linear planning model [J]. Science and Technology Innovation, 2020(28):42-43.

[8] Junsen Wang, JIN Shao-Hua, BIAN Zhi-Gang et al. Residual correction of multibeam bathymetric traverse motion using overlapping regions of neighboring survey lines [J]. Journal of Marine Technology, 2023, 42(04):35-42.

[9] Yingying Fu. Application of multibeam bathymetric system in riverbed change analysis [J]. Urban Road and Bridge and Flood Control, 2023(07):266-269.

[10] Baomao Mu, Xin Ye. Research on Model Predictive Control Strategy Based on Dynamic Programming [J]. Heavy Duty Trucks, 2023, (06): 6-8.